

ALMA OBSERVATIONS OF THE MOLECULAR GAS IN THE DEBRIS DISK OF
THE 30 MYR OLD STAR HD 21997

Á. KÓSPÁL^{1,11}, A. MOÓR², A. JUHÁSZ³, P. ÁBRAHÁM², D. APAI⁴, T. CSENGERI⁵, C. A. GRADY^{6,7}, TH. HENNING⁸, A. M. HUGHES⁹, Cs. KISS², I. PASCUCCI¹⁰, AND M. SCHMALZL³

Draft version July 2, 2018

ABSTRACT

The 30 Myr old A3-type star HD 21997 is one of the two known debris dust disks having a measurable amount of cold molecular gas. With the goal of understanding the physical state, origin, and evolution of the gas in young debris disks, we obtained CO line observations with the Atacama Large Millimeter/submillimeter Array (ALMA). Here we report on the detection of ¹²CO and ¹³CO in the $J=2-1$ and $J=3-2$ transitions and C¹⁸O in the $J=2-1$ line. The gas exhibits a Keplerian velocity curve, one of the few direct measurements of Keplerian rotation in young debris disks. The measured CO brightness distribution could be reproduced by a simple star+disk system, whose parameters are $r_{\text{in}} < 26$ AU, $r_{\text{out}} = 138 \pm 20$ AU, $M_* = 1.8_{-0.2}^{+0.5} M_{\odot}$, and $i = 32^{\circ}6 \pm 3^{\circ}1$. The total CO mass, as calculated from the optically thin C¹⁸O line, is about $(4-8) \times 10^{-2} M_{\oplus}$, while the CO line ratios suggest a radiation temperature on the order of 6–9 K. Comparing our results with those obtained for the dust component of the HD 21997 disk from the ALMA continuum observations by Moór et al., we conclude that comparable amounts of CO gas and dust are present in the disk. Interestingly, the gas and dust in the HD 21997 system are not co-located, indicating a dust-free inner gas disk within 55 AU of the star. We explore two possible scenarios for the origin of the gas. A secondary origin, which involves gas production from colliding or active planetesimals, would require unreasonably high gas production rates and would not explain why the gas and dust are not co-located. We propose that HD 21997 is a hybrid system where secondary debris dust and primordial gas coexist. HD 21997, whose age exceeds both the model predictions for disk clearing and the ages of the oldest T Tauri-like or transitional gas disks in the literature, may be a key object linking the primordial and the debris phases of disk evolution.

Subject headings: circumstellar matter — infrared: stars — stars: individual (HD 21997)

1. INTRODUCTION

Nearly all young stars harbor circumstellar disks whose thermal emission produces a strong infrared excess with fractional luminosities of $L_{\text{d}}/L \geq 0.1$. At the early stage of their evolution, the masses of these disks (typically a few percent of the mass of the central star) are dominated by gas with only a few percent of the mass in small, submicron-sized dust grains. Both the dust and the gas are of primordial origin. As the disk evolves, dust settles in the midplane and the grains eventually form larger

bodies, planetesimals and planets. The gas is removed by viscous accretion (e.g., Lynden-Bell & Pringle 1974), by photoevaporation (e.g., Alexander 2008), or by planet formation. Current observational results imply that the primordial gas is mostly depleted at ages of $\lesssim 10$ Myr (Pascucci et al. 2006; Fedele et al. 2010).

A detectable amount of infrared excess is also present in many older, main-sequence stars, with typical fractional luminosities of $L_{\text{d}}/L \leq 10^{-3}$ (e.g., Roccatagliata et al. 2009). These debris disks are fundamentally different from primordial disks. Their masses, as inferred from the emission of small dust grains, are usually below $1 M_{\oplus}$ and they are practically gas-free. Without the stabilizing effect of surrounding gas, the lifetime of individual dust grains in debris disks is very short due to removal by dynamical interactions with stellar radiation. Thus, dust needs to be continuously replenished by collisions and/or evaporation of previously formed planetesimals (e.g., Wyatt 2008). The same processes would in principle produce gas as well, via sublimation of planetesimals (Lagrange et al. 1998), photodesorption from dust grains (Grigorieva et al. 2007), vaporization of colliding dust particles (Czechowski & Mann 2007), or collision of comets or icy planetesimals (Zuckerman & Song 2012). Thus, the secondary gas that may be present in a debris disk is dominated by CO and H₂O (Mumma & Charnley 2011) and only a small amount of H₂, mainly originating from the dissociation of H₂O, is expected.

¹ European Space Agency (ESA-ESTEC, SRE-SA), P.O. Box 299, 2200AG, Noordwijk, The Netherlands; akospal@rssd.esa.int

² Konkoly Observatory, Research Centre for Astronomy and Earth Sciences, Hungarian Academy of Sciences, P.O. Box 67, 1525 Budapest, Hungary

⁴ Department of Astronomy and Department of Planetary Sciences, The University of Arizona, Tucson, AZ 85721, USA

⁵ Max-Planck-Institut für Radioastronomie, Auf dem Hügel 69, D-53121 Bonn, Germany

⁶ NASA Goddard Space Flight Center, Code 667, Greenbelt, MD 20771, USA

⁷ Eureka Scientific, 2452 Delmer Street, Suite 100, Oakland, CA 94602, USA

⁸ Max-Planck-Institut für Astronomie, Königstuhl 17, D-69117 Heidelberg, Germany

⁹ Astronomy Department, Wesleyan University, Middletown, CT 06459, USA

³ Leiden Observatory, Leiden University, Niels Bohrweg 2, NL-2333 CA Leiden, The Netherlands

¹⁰ Lunar and Planetary Laboratory, Department of Planetary Sciences, University of Arizona, 1629 East University Boulevard, Tucson, AZ 85721, USA

¹¹ ESA Fellow.

In theory, it is possible that systems in transition between the primordial and the debris state possess hybrid disks, i.e. primordial gas is accompanied by secondary dust. It is also possible that the outer disk is still primordial, while the inner disk is already composed of secondary material (Wyatt 2008; Krivov et al. 2009). So far, only six debris disks with detectable gas component are known. The edge-on orientation of the disks around β Pic and HD 32297 allow the detection of a very small amount of circumstellar gas based on the presence of absorption lines (Roberge et al. 2000; Redfield 2007). Another member of the β Pic moving group, HD 172555, also contains some gas as evidenced by [OI] emission at $63\ \mu\text{m}$ (Riviere-Marichalar et al. 2012). Recently, the [CII] line at $158\ \mu\text{m}$ was detected in ~ 30 Myr old HD 32297 (Donaldson et al. 2013). A substantial amount of molecular gas has been detected at millimeter wavelengths in the debris disk around the young main-sequence stars 49 Ceti (Hughes et al. 2008) and HD 21997 (Moór et al. 2011). The age of these systems are between 10 and 40 Myr, which partly overlaps with the transition period from the primordial to the debris phases. Although HD 21997 and 49 Cet are the oldest members of the gaseous debris disk sample, they also contain the largest amount of cold gas. Thus, it is worth considering whether in their case the detected gas is of primordial or secondary origin.

In this paper, we focus on HD 21997, which is an A3-type star at a distance of 72 pc (based on Hipparcos parallax; van Leeuwen 2007), belonging to the well-dated 30 Myr old Columba moving group (Moór et al. 2006; Torres et al. 2008). In an earlier study, we detected molecular gas in the $J=3-2$ and $J=2-1$ transitions (CO(3-2) and CO(2-1)) with the APEX telescope (Moór et al. 2011). Motivated to understand the origin and evolutionary status of the gas component in this system, we obtained (sub)millimeter interferometric continuum and CO line observations with the Atacama Large Millimeter/submillimeter Array (ALMA). Our aim was to spatially resolve the disk in order to study the relative location of the gas and dust components, determine the distribution of the different CO isotopologues, precisely measure the gas mass, and analyze gas kinematics. In this paper, we present our results on the gas content of the disk, while the dust continuum observations are analyzed in Moór et al. (2013, hereafter, Paper I).

2. OBSERVATIONS AND DATA REDUCTION

We observed HD 21997 with ALMA in Cycle 0 using a compact configuration (PI: Á. Kóspál). The quasar J0403-360 served as a bandpass and gain calibrator, while Callisto was used to set the absolute amplitude scale using the CASA Butler-JPL-Horizons 2010 model. We obtained both line and continuum data. Here, we focus on the line observations, while the continuum measurements are presented in Paper I.

In Band 6, we targeted the (2-1) transitions of ^{12}CO , ^{13}CO , and C^{18}O . We used the frequency division correlator mode (FDM). Each of the four simultaneously observed spectral windows offered 3840 channels with a channel separation of 122 kHz, resulting in a bandwidth of 469 MHz per window. The spectral resolution corresponds to a velocity resolution of $0.33\ \text{km s}^{-1}$ at 230 GHz.

Due to restrictions in the setup of the local oscillators, the three CO lines could not be observed simultaneously; therefore, two different correlator configurations were prepared. One setup (A1) was configured to observe $^{13}\text{CO}(2-1)$ and $\text{C}^{18}\text{O}(2-1)$, and it was executed on 2011 November 29 using 14 antennas, with baselines ranging from 9.7 to 148 k λ . The other setup (A2) was tuned to have $^{12}\text{CO}(2-1)$ in one of the spectral windows, and it was observed on 2011 December 31, using 16 antennas, with baselines between 9.6 and 196 k λ . Each of these two setups had an on-source time of 49.4 minutes.

In Band 7, we targeted the (3-2) transitions of ^{12}CO and ^{13}CO , as well as the (7-6) transition of CS. The correlator was set up in FDM with 3840 channels, a channel separation of 244 kHz, and a total bandwidth of 938 MHz. The spectral resolution corresponds to a velocity resolution of $0.44\ \text{km s}^{-1}$ at 345 GHz. Again, two correlator configurations were used. In one setup (B1), $^{12}\text{CO}(3-2)$ and $^{13}\text{CO}(3-2)$ were targeted. Observations were done on 2011 November 3 and 4 using 14 and 15 antennas, respectively, with baselines ranging from 14 to 154 k λ . The other setup (B2) covered the CS(7-6) line, and was observed on 2011 November 3 with 14 antennas and baselines between 14 and 153 k λ . The rest frequency of CS(7-6) also allowed us to obtain additional coverage of $^{13}\text{CO}(3-2)$ in this configuration. Both configurations had an on-source time of 49.4 minutes, resulting in ~ 100 minutes of observing time for $^{13}\text{CO}(3-2)$.

We subtracted the continuum emission in the spectral cubes using the CASA task `uvcontsub`, and individually cleaned the spectral region around each molecular line using the CASA task `clean` with robust weighting. A summary of the observing setup, beam size and position angle (P.A.) for each line, and the rms noise measured in the channel maps is presented in Table 1.

3. RESULTS

3.1. Integrated Line Profiles

We detected all targeted CO lines, i.e., $^{12}\text{CO}(2-1)$, $^{12}\text{CO}(3-2)$, $^{13}\text{CO}(2-1)$, $^{13}\text{CO}(3-2)$, and $\text{C}^{18}\text{O}(2-1)$. Neither the CS(7-6) line nor any other lines are detected in our ALMA data cubes. In order to obtain integrated profiles for the CO lines, we added all the flux within a radius of $2''8$ of the stellar position (the smallest aperture that contains the whole flux of the object) for each velocity channel. The resulting line profiles are plotted in Figure 1 (left panel). In line with our earlier APEX observations (Moór et al. 2011), the lines are all double-peaked, typical for emission arising from rotating material. The intensities of the two ^{12}CO lines are also consistent within the uncertainties with our earlier single-dish APEX results, indicating that there is no significant flux loss due to the interferometer filtering out large-scale structures. The peak and central velocities are the same for all lines. Within the uncertainties, the profiles are symmetric around a systemic velocity of $v_{\text{sys}}=1.29\ \text{km s}^{-1}$ (measured in the local standard of rest (LSR) system), which agrees with the radial velocity of the central star. The intensity-weighted average velocity for all lines is the same ($1.29 \pm 0.05\ \text{km s}^{-1}$) as well. The symmetric profiles suggest that the rotating material is distributed axisymmetrically around the central star.

Table 1 presents the line fluxes integrated from

-4 km s^{-1} to 6.6 km s^{-1} , a velocity interval that covers the whole line, as well as the peak fluxes. The strongest CO line is the 3–2 transition of ^{12}CO , followed by the 2–1 line of the same isotopologue, then the 3–2 and 2–1 transitions of ^{13}CO , while the 2–1 line of C^{18}O is the faintest among our detections. If we normalize the line profiles (Figure 1, right panel), we find that the lines have very similar profiles. We checked which velocity channels contain significant emission above the 3σ level, and found that these span a range of $\pm 4.3 \text{ km s}^{-1}$ around the systemic velocity.

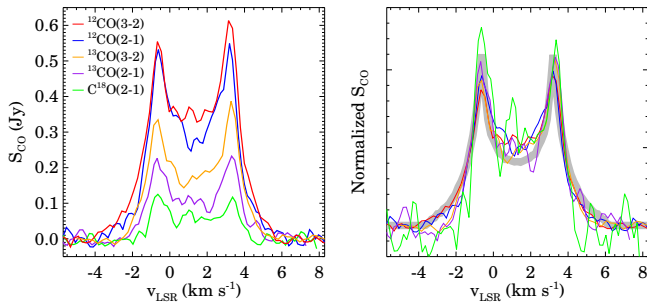


FIG. 1.— CO spectra of HD 21997 observed with ALMA. The left panel shows integrated flux densities in Jy, while the right panel displays spectra normalized to their respective line areas, to better show the similarities in the line profiles. In the right panel, an additional thick gray line shows the best-fit model described in Section 3.4.

3.2. Spatially Resolved CO Emission

The disk was spatially resolved in all CO transitions. We calculated zeroth and first moment maps for each data cube (for an example, see Figure 2, left panel). Figure 2 shows that the intensity profile peaks at the stellar position and smoothly decreases with radial distance. The velocity maps indicate that to the north of the star, material is approaching, while in the south, material is receding, with respect to v_{sys} . The same characteristics can be seen for the other lines as well. Assuming rotating disk kinematics, we can determine the rotation axis by fitting a line to those pixels in the first moment map where the velocity equals to v_{sys} . This axis also marks the minor axis of the inclined disk image. We determined the P.A. of the major axis on each image and obtained on average $22^\circ 6 \pm 0^\circ 5$. The extent of the emission along the minor and major axes defined by the 3σ contour in Figure 2 (left panel) is $3''.5 \times 4''.0$.

Figure 2 (right panel) shows a position velocity diagram measured along the major axis of the disk marked in Figure 2 (left panel). Most of the emission comes from two well-separated regions. The highest velocities are observed closest to the stellar position, and velocity gradually decreases with increasing distance, a pattern characteristic of Keplerian-like disk rotation. In Figure 3 (left panel) we plot the observed CO emission in nine different velocity channels between -3.2 and 3.2 km s^{-1} relative to v_{sys} , in steps of 0.8 km s^{-1} . The plots show that the emission in the most extreme velocity channels is rather compact and is located close to the stellar position. Toward lower velocities, the peak of the emission appears farther from the stellar position. For velocities close to the systemic velocity, the emission is double peaked. The

morphology of the images is very similar on either side of the systemic velocity, apart from a mirroring. It is evident from the plots that the different CO lines exhibit the same emission pattern, allowing for the differences in the beam shape/size and the signal-to-noise ratio.

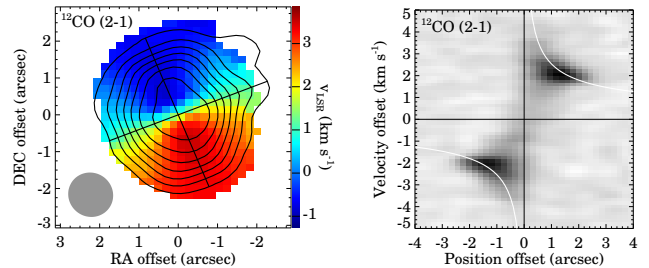


FIG. 2.— Left panel: zeroth moment (with contours) and first moment (with color scale) of the ^{12}CO (2–1) emission. The major and minor axes are plotted with straight black lines. The gray ellipse in the lower left corner indicates the beam. Right panel: position-velocity diagram of ^{12}CO (2–1) emission along the major axis. Overplotted in white is a Keplerian rotation curve for $M_* = 1.8 M_\odot$ and $i = 32^\circ 6$ (see Section 3.4).

3.3. Temperature and Mass of the CO Gas

Despite their very different abundances, the fact that the intensities of the three different CO isotopologues are of the same order of magnitude already indicates that ^{12}CO is probably optically thick. We observed the (2–1) transition for three different CO isotopologues. If we denote the optical depths of ^{12}CO , ^{13}CO , and C^{18}O by τ_{12} , τ_{13} , and τ_{18} , respectively, then the ratio of the ^{12}CO to the C^{18}O line can be approximated as $(1 - e^{-\tau_{12}})/(1 - e^{-\tau_{18}})$ and a similar formula holds for the ^{13}CO to the ^{18}CO line ratio. Assuming that the optical depths of the different isotopologues follow the same proportions as the abundance ratios typical of local interstellar matter (Wilson & Rood 1994), then $\tau_{12} = 560\tau_{18}$, and $\tau_{13} = 7.4\tau_{18}$. Using these numbers, we obtained $\tau_{18} = 0.2$ from the ^{12}CO to the C^{18}O line ratio, and $\tau_{18} = 0.6$ from the ^{13}CO to the C^{18}O line ratio. This result means that τ_{13} is in the 1.5–4.5 range, while τ_{12} is between about 100 and 300. Using comet-like isotopic ratios would yield similar results (Eberhardt et al. 1995; Bockelée-Morvan et al. 2012; Rousselot et al. 2012). According to Visser et al. (2009), and references therein, the $^{12}\text{C}/^{13}\text{C}$ ratio may be a factor of two smaller or larger, while the $^{16}\text{O}/^{18}\text{O}$ ratio may be three to five times larger than the local elemental ratios. This fact means that we may overestimate τ_{13} and τ_{12} by less than a factor of two, or we may underestimate them by as much as a factor of five.

Since the ^{12}CO lines are optically thick, the ALMA $^{12}\text{CO}(2-1)$ and $^{12}\text{CO}(3-2)$ maps can be used to calculate the radiation temperature of the gas by comparing the observed surface brightness with a blackbody. For optically thick lines, the radiation temperature equals the excitation temperature. Because the intrinsic line width and the significant macroscopic movements of the gas as it orbits the central star decrease the optical depth at a certain frequency, we always selected the frequency channel with the maximal intensity for each map pixel. This way, for each map pixel, we can estimate the tem-

TABLE 1
REST FREQUENCIES, OBSERVING SETUPS (SEE TEXT FOR DETAILS), BEAM SIZES AND POSITION ANGLES, NOISE LEVELS, AND LINE FLUXES FOR THE CO OBSERVATIONS OF HD 21997

Line	Frequency (GHz)	Setup	Beam Size (″×″)	Beam PA (°)	Noise (mJy beam ⁻¹ channel ⁻¹)	Peak Flux (Jy)	Total Flux (Jy km s ⁻¹)	Total Flux (W m ⁻²)
¹² CO(3–2)	345.796	B1	1.19×1.47	117.5	7.9	0.615	2.52 ± 0.27	(2.91 ± 0.31) × 10 ⁻²⁰
¹² CO(2–1)	230.538	A2	1.14×1.21	16.4	8.6	0.566	2.17 ± 0.23	(1.67 ± 0.18) × 10 ⁻²⁰
¹³ CO(3–2)	330.588	B1, B2	1.20×1.38	-49.9	5.7	0.387	1.35 ± 0.15	(1.49 ± 0.17) × 10 ⁻²⁰
¹³ CO(2–1)	220.399	A1	1.19×1.92	19.0	7.6	0.238	0.82 ± 0.10	(6.04 ± 0.74) × 10 ⁻²¹
C ¹⁸ O(2–1)	219.560	A1	1.21×1.92	18.6	9.0	0.129	0.36 ± 0.06	(2.63 ± 0.44) × 10 ⁻²¹

perature at the frequency (or velocity) where the optical depth is the highest. For ¹²CO we obtained excitation temperatures up to 9 K. The temperature can also be estimated from the ratio of the optically thick ¹²CO(3–2) and ¹²CO(2–1) lines. In the Rayleigh-Jeans approximation, the ratio is expected to be the ratio of the squares of the line frequencies, i.e. about 2.25. Instead, using the total flux values from Table 1, we obtain 1.16. The low value suggests that the temperature is very low and that the Rayleigh-Jeans approximation is not valid. Indeed, using the Planck function, it turns out that these line ratios correspond to 5.6 K.

In Moór et al. (2011), given a lack of more information, we assumed that ¹²CO was optically thin and estimated a total CO mass of $3.5 \times 10^{-4} M_{\oplus}$. Our ALMA observations made it evident that ¹²CO was optically thick and that C¹⁸O should be used for mass estimation. The calculations depend on the temperature of the gas, for which we used different values between 5.6 K (the excitation temperature obtained from the ¹²CO (3–2) to (2–1) line ratio) and 100 K (the hottest dust temperatures at the inner edge of the disk in the model of Paper I). Higher temperatures mean higher emission, but also mean that these low- J transitions are less excited. The net result of these two effects is that within the assumed temperature range, the total CO mass needed to produce the observed emission changes by only a factor of two. Thus, the CO mass is well constrained, even without knowing the precise temperature. The resulting value, $(4\text{--}8) \times 10^{-2} M_{\oplus}$, is about two orders of magnitude higher than previously believed. Considering the uncertainties in the ¹²CO, ¹³CO and C¹⁸O isotopic ratios mentioned above, the total CO mass may actually be a factor of two smaller or a factor of five higher than this value. Nevertheless, the precise value does not change the fact that HD 21997 has an unusually gas-rich disk.

If the gas has a second-generation origin, the most common species, based on cometary composition, are H₂O, CO, and CO₂ in comparable abundances (Mumma & Charnley 2011, and references therein). Thus, the CO mass gives a good estimate for the order of magnitude of the total gas mass in the disk. However, if the gas is primordial, then not only CO but also H₂ gas is present in the disk and the total gas mass is significantly higher. Taking a canonical CO/H₂ abundance ratio of 10^{-4} , the total gas mass is on the order of 26–60 M_{\oplus} . If such a large amount of H₂ is indeed present, and it is warm enough, the gas should display rotational lines at mid-infrared wavelengths. We checked the *Spitzer*/Infrared Spectrograph spectrum of HD 21997 (Paper I) for the $S(0)$, $S(1)$, and $S(2)$ lines, but found that they are not present. Using a 3σ upper limit for

TABLE 2
PARAMETERS OF THE HD 21997 SYSTEM AND ITS GAS DISK

Distance	d (pc)	71.95
Systemic velocity	v_{LSR} (km s ⁻¹)	1.29
Disk orientation	$P.A.$ (°)	22.6 ± 0.5
Disk inner radius	r_{in} (AU)	< 26
Disk outer radius	r_{out} (AU)	138 ± 20
Stellar mass	M_* (M_{\odot})	1.8 ^{+0.5} _{-0.2}
Disk inclination	i (°)	32.6 ± 3.1
Disk brightness exponent	p	-1.1 ± 1.4

the flux of the line expected to be the brightest, $S(0)$, we calculated an upper limit of 35 M_{\oplus} for the total gas mass for 100 K gas and 3400 M_{\oplus} for 50 K gas. This result means that even if H₂ is present, it should be quite cold, just like the CO gas.

3.4. Distribution of the CO Gas

To determine the basic parameters of the HD 21997 gas disk, we fit the spatial and velocity distributions of the observed CO emission with a simple disk geometry combined with a Keplerian velocity profile. Our simple model has five parameters: the stellar mass (M_*), the inner and outer disk radii (r_{out} , r_{in}), the inclination of the disk (i , where $i=0^\circ$ corresponds to face on), and the exponent (p) of the radial brightness profile, assumed to be a power law ($I(r) \propto r^p$). For the velocity field of the gas, we adopted Keplerian rotation around the central star, expected to be true for low-mass, non-self-gravitating disks (e.g., Dutrey et al. 2007). We used an intrinsic line width of 0.1 km s⁻¹, corresponding to the Doppler broadening of a line arising from ≈ 10 K gas. We calculated the models for the same velocity channels as the actual observations and applied a two-channel wide Hanning smoothing to account for the instrumental velocity resolution. In the spatial direction, we first calculated the models with a 6× oversampling, convolved the models with the beam of the actual observations, and rebinned them to the same pixel scale as the observations. We decided to model the ¹²CO (2–1) line, which is one of the brightest we observed and has the smallest and most circular beam.

To explore a sufficiently large parameter range, we changed M_* between 0.9 M_{\odot} and 3.0 M_{\odot} in steps of 0.3 M_{\odot} , r_{in} between 5 AU and 60 AU in steps of 5 AU, r_{out} between 95 AU and 175 AU in steps of 5 AU, i between 25° and 39° in steps of 2°, and p between 0 and -1.75 in steps of 0.25. In total, we calculated 104,448 models. In order to compare the models with the observations, we normalized the models so that the total intensity equaled the observed total intensity. Then, we

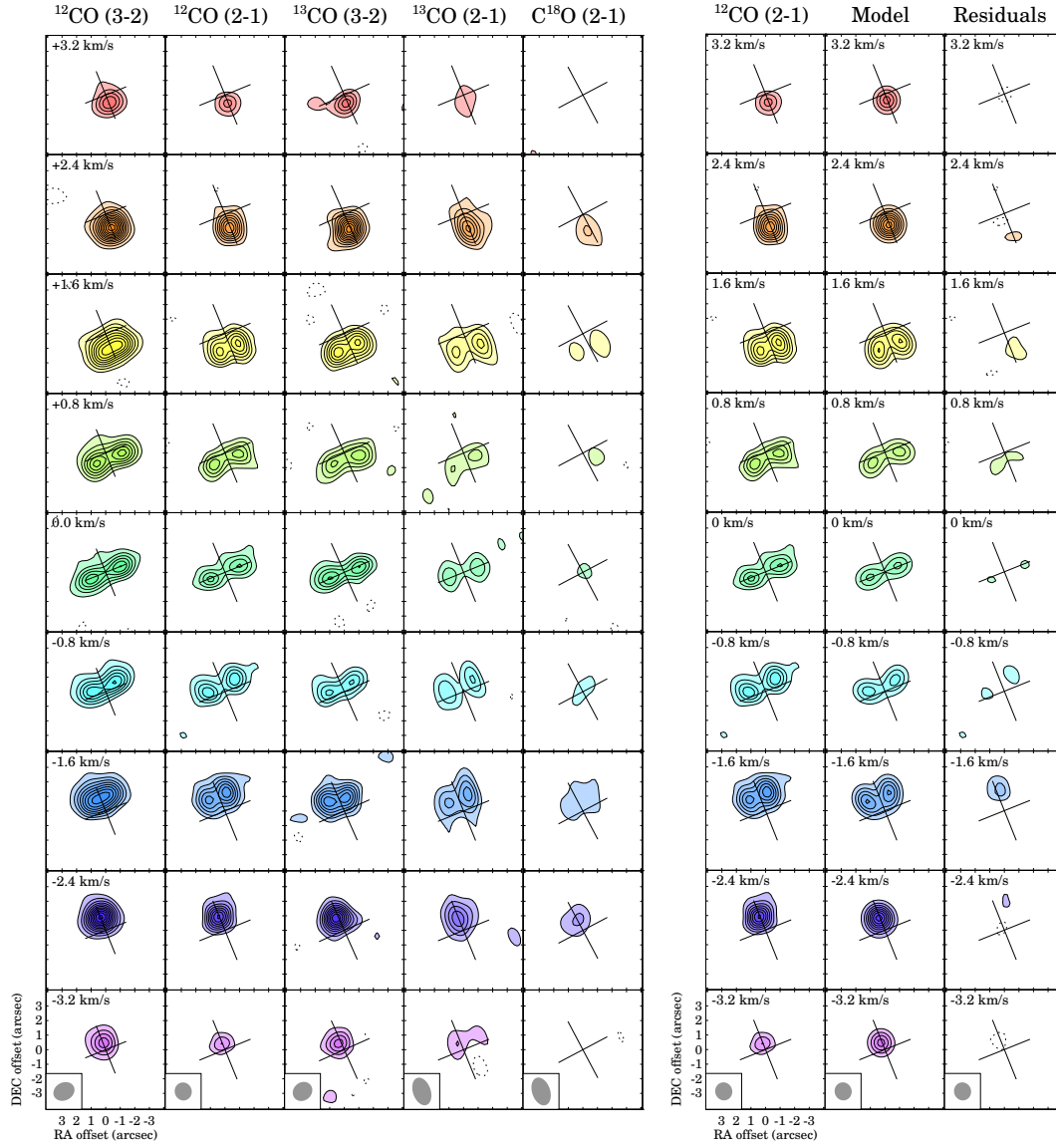


FIG. 3.— Left: channel maps of CO observations of HD 21997. Velocities indicated in the upper left corners are relative to the systemic velocity. Solid contours mark the 3σ , 6σ , 9σ , 12σ , etc... levels, while dashed contours indicate the -3σ level. Right: observed and modeled CO channel maps for the ^{12}CO (2–1) line, and residuals. Details of the model are described in Section 3.4. Contours are the same as in the left panel.

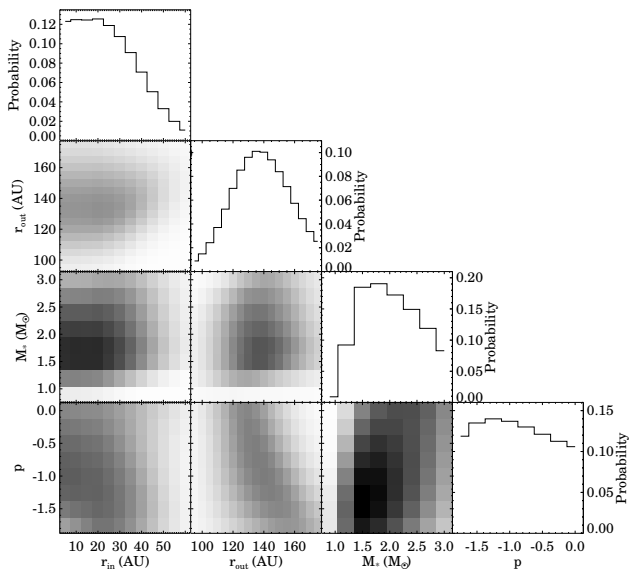


FIG. 4.— Marginal probability distribution for the different model parameters. Details of the model are described in Section 3.4.

computed the χ^2 for each channel map. The final χ^2 of a certain model was defined as the maximum of the χ^2 of all channels. Finally, we calculated the Bayesian probability for each model as $\exp(-\chi^2/2)$ and normalized them so that the sum of the probabilities of all models is 1. Figure 4 shows the one-dimensional (1D) probability distributions as a function of each parameter, and the two-dimensional (2D) probability distributions as a function of two different parameters. These are marginal distributions, i.e., for example, in the distribution as a function of r_{in} , all the other parameters (r_{out} , M_* , i , and p) were marginalized out. Similarly, for example, in case of the 2D distribution for r_{in} and r_{out} , M_* , i , and p were marginalized out (for more information on Bayesian inference and marginalization, see, e.g., Loredo 1992). The value where the 1D probability distribution is maximal formally gives the best estimate for that parameter. Formal 1σ uncertainties can also be estimated from these graphs by integrating the probability distributions on each side of the maximum until one obtains 0.68. However, it is evident from Figure 4 that not all parameters are equally well determined. The probability distribution as a function of r_{in} is quite flat for short inner radii, indicating that we can only give an upper limit on r_{in} . The outer radius r_{out} and stellar mass M_* are well determined, while the power-law exponent of the brightness profile, p , shows a very slowly changing and wide probability distribution, which practically makes this parameter ill-determined. The inclination and the stellar mass are degenerate, thus we did not determine the inclination from the Bayesian probabilities, but calculated it directly from the best-fit stellar mass.

Table 2 shows our best estimates for the disk parameters and their 1σ uncertainties, along with a 1σ upper limit for r_{in} . Figure 3 (right panel) shows side-by-side the channel maps for the ^{12}CO (2–1) observations, the

model with the best parameters (and $r_{\text{in}}=20$ AU), as well as the residuals. Moreover, we plotted the integrated line profile from the model in Figure 1. These figures demonstrate that the best model we found indeed fits the channel maps and line profile very well. We convolved this model with a beam appropriate for our other CO observations and scaled them so that the integrated line intensity equals the observed intensities. We then plotted the channel maps and residuals similarly to those in Figure 3 (right panel) and found that the observations and the model match each other well. This fact demonstrates that a single disk model with one set of parameters reproduces all five CO lines.

In the following, we check whether the fitted parameters are consistent with our a priori expectations. The major axis of the ^{12}CO (2–1) image is $4''.0$ (Section 3.2), which, deconvolved with the beam size of $1''.21$ (Table 1), gives an outer radius of 137 AU, in agreement with our fitted value. We can estimate the inclination from the ratio of the minor and major axes of the ^{12}CO (2–1) image, which gives 29° (cf. $32.6^\circ \pm 3.1^\circ$ in Table 2). A similar calculation was done from the minor and major axes of the ellipse fit to the ALMA dust continuum image (Paper I), giving $32.9^\circ \pm 2.6^\circ$. Another argument in favor of a $\approx 30^\circ$ inclination is that from the measured $v \sin i = 70 \text{ km s}^{-1}$ (Royer et al. 2007), we obtain an equatorial rotational velocity of 140 km s^{-1} , typical for A-type stars with a mass of about $1.8 M_\odot$ (Zorec & Royer 2012). Finally, the dynamical stellar mass of $1.8 M_\odot$ agrees well with the mass of $1.85 M_\odot$ obtained from evolutionary tracks by Moór et al. (2011). These comparisons demonstrate that our simple fitting procedure provided reasonable results for the basic properties of the CO gas distribution. A more detailed physical model, taking into account the vertical disk structure and full radiative transfer, is postponed to our forthcoming paper.

4. DISCUSSION

Our modeling in Section 3.4 suggests that the observed CO emission can be well described by a gas disk in Keplerian rotation around a $1.8 M_\odot$ central star. For the inner radius of the gas disk, we obtained a 1σ upper limit of 26 AU. In Paper I, we found that the dust disk starts at a radius of ≈ 55 AU. Consequently, we can claim with a 99% confidence that the inner radius of the gas is closer to the central star than that of the dust disk. This result is in accordance with the strikingly different appearance of the ring-like dust continuum image and the centrally-peaked CO zeroth moment maps. There is a part in the disk where the gas and the dust are not co-located and this “inner disk” is practically dust-free. The total CO gas mass is about $(4\text{--}8) \times 10^{-2} M_\oplus$. In Paper I, we modeled the dust emission of HD 21997, and found that the dust mass within about 150 AU is $0.09 M_\oplus$, resulting in a CO-to-dust ratio of 0.4–0.9, i.e., roughly the same mass of dust and CO gas is present in the disk. This value may actually be slightly lower if we take into account that a fraction of the gas is located in the inner dust-free area. While the dust properties of the HD 21997 system are characteristic of a typical debris disk (Paper I), there is an unexpectedly large amount of gas in the disk (for comparison, the CO-to-dust ratio in β Pic is less than 2×10^{-4} ; Dent et al. 1995; Nilsson et al.

2009). In the following, we discuss different possibilities for the origin, physical properties, and possible evolution of the gas component.

4.1. Debris Disk with Pure Secondary Gas

In a debris disk, where neither dust grains nor H_2 provide enough shielding for CO, the main factor determining the CO lifetime is its self-shielding against the stellar UV radiation field and the interstellar radiation field. To estimate the CO lifetime in the HD 21997 disk, we distributed the measured CO mass between 20 AU and 138 AU, adopted a power-law radial density distribution ($n \propto r^{-\alpha}$, with $\alpha = 1.5, 2.0,$ and 2.5), and assumed three different vertical scale heights ($H/r = 0.05, 0.1,$ and 0.2). We computed the radial and vertical column density of CO in the disk and estimated the shielding factors for ^{12}CO and C^{18}O from the tabulated values of Visser et al. (2009). We neglected the shielding from the dust grains due to their low column density. We took into account both stellar UV flux and the interstellar radiation field, the same way as in Moór et al. (2011). The resulting lifetimes are below 30,000 yr for ^{12}CO , and below 6000 yr for C^{18}O . The Keplerian rotation of the gas and resulting Doppler shift of the line would further decrease the optical depth and reduce the lifetime. Thus, a replenishment of CO molecules is needed.

Assuming an equilibrium between the dissociation and production of CO molecules, and dividing the measured gas mass by the maximum lifetime computed for ^{12}CO , we obtained a lower limit for the gas production rate of about $10^{19} \text{ kg yr}^{-1}$ (approx. $10^{-6} M_{\oplus} \text{ yr}^{-1}$). We emphasize that this production rate is a very optimistic lower limit, because for a significant part of the disk, CO lifetimes are lower than the value quoted above. Typical gas production rates in solar system comets are on the order of $10^9\text{--}10^{10} \text{ kg yr}^{-1}$ (Wyckoff 1982). Most of this gas, however, is H_2O , and CO production is lower by a factor of 5–100 (Jewitt et al. 2007). This fact means that to keep up the observed CO mass in HD 21997, the continuous gas production of $10^{10}\text{--}10^{11}$ comets is needed. Alternatively, considering a larger comet like Hale–Bopp (total mass of $1.3 \times 10^{16} \text{ kg}$; Weissman 2007) and assuming a $\sim 10\%$ CO content (Sykes et al. 1986; Mumma & Charnley 2011), at least 6000 Hale–Bopp-like comets need to be completely destroyed every year. Unless one assumes a recent transient event in which a large amount of CO was produced, the calculated very high replenishment rate argues against the secondary origin of the CO gas in the HD 21997 system.

The destruction of planetesimals may result in both debris dust and secondary gas (Section 1). If the gas and dust indeed have a common origin in the HD 21997 system, one would expect that they are co-located, unless some physical process separates gas and dust and moves the gas inward or the dust outward from where they were produced. One possibility is that the planetesimal ring starts about 55 AU from the star, as the location of the dust disk implies. Viscous accretion can transport material into the inner part, but it would act both on gas and the small dust particles. The other possibility would be to assume that the gas production via the destruction of comets occurs in the warm inner disk. However, comets would also produce dust, which was not observed. Thus, the existence of the dust-free gas disk

cannot be explained in the secondary scenario.

4.2. Primordial Gas in a Hybrid Disk

The other possible scenario for the origin of the gas in the HD 21997 system is that the CO molecules are remnants of the primordial protoplanetary disk. Their survival would require very efficient shielding over the 30 Myr long history of the system. Attributing this shielding to the presence of H_2 gas (with a CO/H_2 abundance ratio of 10^{-4}) and distributing the H_2 in the same simple disk geometry as we assumed for the CO in Section 4.1, we found CO lifetimes typically two orders of magnitude longer than without the presence of H_2 , long enough that some primordial gas can still be present in the system. There is, however, one important drawback of the primordial gas scenario. The calculation above shows that the H_2 number density in the midplane is high enough ($n_{\text{H}_2} > 10^6 \text{ cm}^{-3}$) for the CO gas to be collisionally excited and be in local thermodynamic equilibrium (LTE), using the critical densities from Kamp & van Zadelhoff (2001). In this case, the excitation temperature equals the kinetic temperature. Our CO observations indicate very low excitation temperatures, much lower than the dust temperature (64 K, based on spectral energy distribution fitting done by Moór et al. 2011). It is an open question what could cause such a difference. The relatively warm dust temperature explains why the CO does not freeze out onto the dust grains.

The oldest phases in primordial disk evolution are represented by transitional disks. From a morphological point of view, HD 21997 might give the impression of a transitional disk where gas exists within the dust-free hole (for such examples, see Brown et al. 2009 or Casassus et al. 2013). However, we argue that HD 21997 is not a transitional disk because our results indicate that its dust content is debris-like. This conclusion is supported by the following: (1) in transitional disks, the gas-to-dust ratio is typically below the interstellar value of 100 (Keane et al. 2013), while in HD 21997, using the total gas mass including H_2 , this ratio would be in the order of 300–700. This result suggests that HD 21997 is unusually dust-poor, possibly because the majority of the dust is already locked up in planetesimals. (2) The dust mass is only $0.1 M_{\oplus}$, significantly lower than typical for transitional disks. (3) There are no spectral signatures of small particles, either silicates or polycyclic aromatic hydrocarbons. (4) The limited lifetime of dust particles even in the presence of gas requires replenishment (Paper I).

Based on these arguments, it is possible that we detected a hybrid system where the gas is primordial while the dust is already secondary. This result would also explain why the dust and gas are not co-located. Because the dust component of HD 21997 consists of large grains ($> 6 \mu\text{m}$; Paper I), the grains trace the location of the planetesimal belt starting at about 55 AU. The gas, however, is the remnant of the primordial circumstellar material and thus may fill the full disk. It is interesting to speculate about the further evolution of the gas component in this system. It may be a stable structure, or it may be in the phase of final disappearance. We note that there are still unresolved issues with the hybrid disk scenario. What happened to the primordial dust in the central dust-free inner disk? Planetesimals already formed

in the outer disk, as evidenced by the debris dust, but why are they missing in the inner disk where dynamical timescales are shorter? Is it possible that solids rapidly accreted to planet masses without affecting the gas component (by forming super-Earths rather than Jupiters)? The future discovery of similar hybrid systems may help to answer these questions. Some of the answers may also help to better understand the evolution of some transitional disks, where the central clearing may contain tenuous secondary dust, while the outer disks consist of primordial gas and dust.

5. SUMMARY AND CONCLUSIONS

We presented ALMA CO line observations of the disk around the 30 Myr old star HD 21997. We detected the (2–1) and (3–2) lines of ^{12}CO and ^{13}CO , and the (2–1) line of C^{18}O . The line profiles and channel maps show that the gas is in Keplerian rotation around the central star. We calculated a grid of simple gas disk models with varying inner and outer radii, inclinations, stellar masses, and radial brightness profiles of CO emission. Using Bayesian probability analysis, we found that the best model gives $r_{\text{in}} < 26$ AU, $r_{\text{out}} = 138$ AU, $M_* = 1.8 M_{\odot}$, and $i = 32^{\circ}6$, while the brightness profile is undetermined. The CO line ratios and intensities suggest that the gas temperature is very low (on the order of 6–9 K). The total CO mass in the disk, as calculated from the optically thin C^{18}O line, is about $(4\text{--}8) \times 10^{-2} M_{\oplus}$. Comparing our results with those obtained for the dust component from the ALMA continuum observations in Paper I, we concluded that, in terms of mass, a similar amount of CO gas and dust is present in the disk. Interestingly, the gas and dust in the HD 21997 system are not co-located: there is an inner, dust-free gas disk extending from closer than about 26 AU to about 55 AU from the star.

We discussed two possible scenarios for the origin of the gas in the HD 21997 disk. First we explored the possibility that the gas is of secondary origin, mainly CO produced by planetesimals. In this case, the sub-critical gas densities would lead to non-LTE conditions, which might explain the low excitation temperatures. However, the short CO lifetimes and the necessary high CO production rates exclude this scenario. The other possibility is that the gas is primordial. In this case, there is a large amount of H_2 gas in the disk, leading to significantly longer CO lifetimes. A primordial origin would explain the different locations of the gas and the dust. Based on our ALMA observations, we propose that HD 21997 is a hybrid system, where primordial gas is accompanied by secondary debris dust. This fact challenges the current paradigm of disk evolution, because the age of HD 21997 exceeds both the model predictions for disk clearing and the ages of the oldest T Tauri-like or transitional gas disks in the literature (Kastner et al. 2008).

We thank the anonymous referee for useful comments that helped us to improve the manuscript. This paper makes use of the following ALMA data: ADS/JAO.ALMA#2011.0.00780.S. ALMA is a partnership of ESO (representing its member states), NSF (USA) and NINS (Japan), together with NRC (Canada) and NSC and ASIAA (Taiwan), in cooperation with the Republic of Chile. The Joint ALMA Observatory is operated by ESO, AUI/NRAO and NAOJ. This work was partly supported by the grant OTKA-101393 of the Hungarian Scientific Research Fund. This work is based in part on observations made with *Herschel*, a European Space Agency Cornerstone Mission with significant participation by NASA. Support for this work was provided by NASA through an award issued by JPL/Caltech.

Facility: ALMA.

REFERENCES

- Alexander, R. D. 2008, MNRAS, 391, L64
 Bockelée-Morvan, D., Biver, N., Swinyard, B., et al. 2012, A&A, 544, L15
 Brown, J. M., Blake, G. A., Qi, C., et al. 2009, ApJ, 704, 496
 Casassus, S., van der Plas, G., M, S. P., et al. 2013, Nature, 493, 191
 Czechowski, A., & Mann, I. 2007, ApJ, 660, 1541
 Dent, W. R. F., Greaves, J. S., Mannings, V., Coulson, I. M., & Walther, D. M. 1995, MNRAS, 277, L25
 Donaldson, J. K., Lebreton, J., Roberge, A., Augereau, J.-C., & Krivov, A. V. 2013, ApJ, 772, 17
 Dutrey, A., Guilloteau, S., & Ho, P. 2007, Protostars and Planets V, 495
 Eberhardt, P., Reber, M., Krankowsky, D., & Hodges, R. R. 1995, A&A, 302, 301
 Fedele, D., van den Ancker, M. E., Henning, T., Jayawardhana, R., & Oliveira, J. M. 2010, A&A, 510, A72
 Grigorieva, A., Thébault, P., Artymowicz, P., & Brandeker, A. 2007, A&A, 475, 755
 Hughes, A. M., Wilner, D. J., Kamp, I., & Hogerheijde, M. R. 2008, ApJ, 681, 626
 Jewitt, D., Chizmadia, L., Grimm, R., & Prialnik, D. 2007, Protostars and Planets V, 863
 Kamp, I., & van Zadelhoff, G.-J. 2001, A&A, 373, 641
 Kastner, J. H., Zuckerman, B., Hily-Blant, P., & Forveille, T. 2008, A&A, 492, 469
 Keane, J. T., Pascucci, I., Andrews, S. M., et al. 2013, in American Astronomical Society Meeting Abstracts, Vol. 221, American Astronomical Society Meeting Abstracts, 220.02
 Krivov, A. V., Herrmann, F., Brandeker, A., & Thébault, P. 2009, A&A, 507, 1503
 Lagrange, A.-M., Beust, H., Mouillet, D., et al. 1998, A&A, 330, 1091
 Lored, T. J. 1992, in Statistical Challenges in Modern Astronomy, ed. E. D. Feigelson & G. J. Babu, 275–306
 Lynden-Bell, D., & Pringle, J. E. 1974, MNRAS, 168, 603
 Moór, A., Ábrahám, P., Derekas, A., et al. 2006, ApJ, 644, 525
 Moór, A., Ábrahám, P., Juhász, A., et al. 2011, ApJ, 740, L7
 Moór, A., et al. 2013, ApJ
 Mumma, M. J., & Charnley, S. B. 2011, ARA&A, 49, 471
 Nilsson, R., Liseau, R., Brandeker, A., et al. 2009, A&A, 508, 1057
 Pascucci, I., Gorti, U., Hollenbach, D., et al. 2006, ApJ, 651, 1177
 Redfield, S. 2007, ApJ, 656, L97
 Riviere-Marichalar, P., Barrado, D., Augereau, J.-C., et al. 2012, A&A, 546, L8
 Roberge, A., Feldman, P. D., Lagrange, A. M., et al. 2000, ApJ, 538, 904
 Roccatagliata, V., Henning, T., Wolf, S., et al. 2009, A&A, 497, 409
 Rousselot, P., Jehin, E., Manfroid, J., & Hutsemékers, D. 2012, A&A, 545, A24
 Royer, F., Zorec, J., & Gómez, A. E. 2007, A&A, 463, 671
 Sykes, M. V., Lebofsky, L. A., Huntten, D. M., & Low, F. 1986, Science, 232, 1115
 Torres, C. A. O., Quast, G. R., Melo, C. H. F., & Sterzik, M. F. 2008, Young Nearby Loose Associations, ed. B. Reipurth, 757
 van Leeuwen, F. 2007, A&A, 474, 653
 Visser, R., van Dishoeck, E. F., & Black, J. H. 2009, A&A, 503, 323
 Weissman, P. R. 2007, in IAU Symposium, Vol. 236, IAU Symposium, ed. G. B. Valsecchi, D. Vokrouhlický, & A. Milani, 441–450
 Wilson, T. L., & Rood, R. 1994, ARA&A, 32, 191
 Wyatt, M. C. 2008, ARA&A, 46, 339

Wyckoff, S. 1982, in IAU Colloq. 61: Comet Discoveries,
Statistics, and Observational Selection, ed. L. L. Wilkening,
3-55
Zorec, J., & Royer, F. 2012, A&A, 537, A120

Zuckerman, B., & Song, I. 2012, ApJ, 758, 77